AIAA Atmospheric Flight Mechanics Conference and Exhibit
18 - 21 August 2008, Honolulu, Hawaii

AIAA 2008-6383

Canard-Elevon Interactions on a Hypersonic Vehicle

Michael W. Oppenheimer *
Torstens Skujins †
David B. Doman ‡
Carlos E. S. Cesnik §

I. Abstract

Hypersonic vehicles are typically characterized by long, slender bodies with highly coupled engine and airframe. For a case where the engine is underslung (below the center-of-gravity), a large elevon control surface is typically necessary to trim the vehicle. The elevon is usually placed at the rear of the vehicle to yield a large moment arm. One issue with tail controlled aircraft is that they exhibit non-minimum phase behavior with respect to flight path angle. Due to the large size of the elevon for some hypersonic vehicles, a deflection of this surface causes a large perturbation to the lift on the vehicle. Additional control effectors can be used to counteract this adverse effect and, in many cases, canards are added to the vehicle to not only aid in increasing the frequency of the non-minimum phase zero, but also to provide improved low-speed handling. By adding a control surface forward of another, there is the potential for an interaction between control effectors, that is, the deflection of the forward surface causes changes to the effectiveness of the rearward surface. In this work, the interaction effects between a canard and elevon are calculated for a generic hypersonic vehicle. The result is a change in the effectiveness of the elevon caused by actual flow on the elevon being different than freestream flow.

II. Introduction

In recent years, there has been a renewed interest in hypersonic flight. In the 1980's, the National Aerospace Plane (NASP) program commenced, with its goal being a feasibility study for a single-stage to orbit (SSTO) vehicle. It was expected to be reusable and could take off and land horizontally. The NASP was to be powered by a supersonic combustion ramjet (scramjet) engine. Although this program was cancelled in the 1990's, a great deal of knowledge was gained and it spawned future programs, including the hypersonic systems technology program (HySTP), initiated in late 1994, and the NASA X-43A. The HySTP's goal was to transfer the accomplishments of the NASP program to a technology demonstration program. This program was cancelled in early 1995. The NASA X-43A set new world speed records in 2004, reaching Mach 6.8 and Mach 9.6 on two separate occasions with a scramjet engine. These flights were the culmination of NASA's Hyper-X program, with the objective being to explore alternatives to rocket power for space access vehicles.

Designing effective controllers for air-breathing hypersonic vehicles requires reliable characterization of the vehicle's unique dynamics. These dynamics come from the strong interactions between aerodynamics, elastic airframe and control effector deformations, heat transfer, and the propulsion system (itself tightly integrated into the lifting body). The accurate characterization of the flight dynamics of such vehicles is

*Electronics Engineer, Control Analysis and Design Branch, 2210 Eighth Street, Bldg. 146, Rm. 305, Air Force Research Laboratory, WPAFB, OH 45433-7531, Email Michael.Oppenheimer@wpafb.af.mil, Ph. (937) 255-8490, Fax (937) 656-4000, Senior Member AIAA

†Graduate Student, University of Michigan, Email tskujins@umich.edu, Ph. (937) 271-3455, Student Member AIAA

‡Senior Aerospace Engineer, Control Analysis and Design Branch, 2210 Eighth Street, Bldg. 146, Rm. 305, Air Force Research Laboratory, WPAFB, OH 45433-7531, Email David.Doman@wpafb.af.mil, Ph. (937) 255-8451, Fax (937) 656-4000, Senior Member AIAA

§Associate Professor of Aerospace Engineering, University of Michigan, Email cesnik@umich.edu, Ph. (734) 764-3397, Associate Fellow AIAA

difficult. Additional complexity is introduced when there exists aerodynamic coupling between a control surface upstream of another. In this work, the effects of a canard on the downstream elevon control surface are considered.

In addition to having an elevon located on the aftbody, a hypersonic vehicle may have a canard on the forebody. The purpose of the canard is twofold: 1. To generate pitching moments in conjunction with the elevon while maintaining a zero net change in lift and 2. To aid in low-speed handling by allowing changes in pitching moment without losing lift. Because it is desired to balance the lift of the canard and elevon, while producing a commanded pitching moment, it is important to determine the aerodynamic effects of the canard on the elevon.

Limited research has been performed on this problem. The two main studies of the flow conditions at the trailing edge of a two-dimensional supersonic airfoil were presented by Kahane[1] and Lighthill.[2] Lighthill built upon the work of Busemann,[3] who developed a power series method to determine the pressures behind shock waves and expansion fans, and used it to study the flow just behind a flat plate airfoil. Behind the trailing edge, the pressures of the flow from the top and bottom of the plate must be equal. Lighthill used Busemann's power series method to equate these pressures, resulting in the flow leaving the flat plate at an angle which is different from the original angle of attack. However, in his analysis, as pointed out by Kahane,[1] he only considered the isentropic terms of the series.

The goal of this work is to calculate the interaction effects between a canard and an elevon. To do so requires calculation of the flow properties on the downstream surface, namely, the elevon. From a controls perspective, the objective is to determine the force and moment generating capabilities of the elevon and hence, the elevon effectiveness. The flow properties at the trailing edge of the canard are calculated using two techniques. The first utilizes Busemann's[3] series method, which, as will be seen, is accurate only for small flow turning angles. The second is a numerical technique developed in this work to balance the pressures on the top and bottom of the trailing edge of a flat plate. This provides a new flow turning angle, which, in general, is different than the leading edge turning angle. Additionally, the flow just downstream of the trailing edge of the canard is assumed to be the incident flow on the elevon. A comparison between elevon effectiveness with and without the upstream effects is provided.

Figure 1 shows the two-dimensional hypersonic vehicle considered in this work.[4] The locations of the canard and elevon are shown and the distance between the control effectors is 70 ft. Both the canard and elevon are modelled as flat plates hinged at their midpoints. In characterizing the two-dimensional

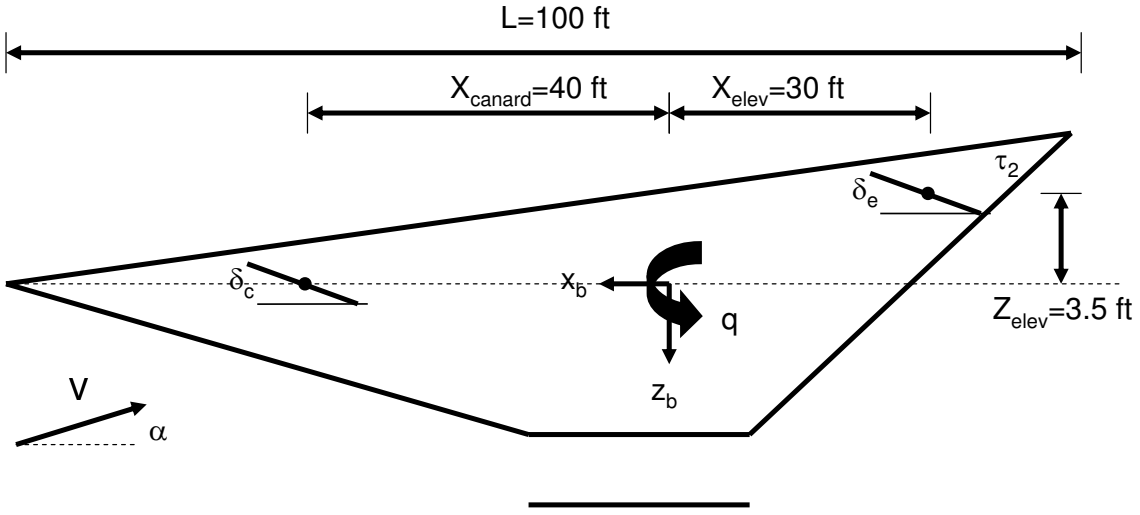

Figure 1. Hypersonic Vehicle.

interaction effects here, a few assumptions are made. First, the flow properties at the elevon are the same as the flow properties at the trailing edge of the canard. In other words, no mixing between the canard flow and freestream flow occur. This is a worst case situation. Second, interaction effects between shocks and expansion fans are ignored. Such interaction structures are complicated and are not easily described by the

use of analytical methods. Additionally, the flow is assumed to be inviscid and the ratio of specific heats is a constant. Other interactions of shocks and expansion fans as well as three-dimensional interactions from both the control surfaces and the body may play significant roles in the vehicle dynamics, but are beyond the scope of this paper. Therefore, the goals of this paper are to present an efficient numerical algorithm, which calculates canard and elevon flow properties, that can be eventually used in a simulation of a complete hypersonic vehicle and to assess the aerodynamic impact that the presence of the canard has on the control effectiveness of an elevon.

III. Flow Behind the Canard

Consider a supersonic flow over a flat plate with angle of attack α with respect to the flow and a canard deflection angle δ_c, as shown in Figure 2. When $\delta_c > -\alpha$, flow on the top side of the front of the plate will pass through a Prandtl-Meyer expansion fan, which will increase the Mach number while decreasing the pressure. The flow on the bottom will pass through an oblique shock, which decreases the Mach number and increases the pressure. At this point, the flow on both sides of the flat plate is parallel to the surface (canard). At the trailing edge, the streams are deflected so that they are again parallel to each other. The flow over the top will pass through an oblique shock while the flow on the bottom will pass through an expansion fan. The critical aspect here is that the flow direction downstream of the trailing edge is no longer parallel to the freestream flow. In fact, there is a surface of slip (or slipstream) between the flow coming from above and below the canard. The pressure in the regions above and below the slipstream are identical; however, the velocity, density, temperature, and entropy differ. One of the goals of this work is to determine the flow direction aft of the canard, relative to the body x-axis, denoted by α'. At the trailing edge, the

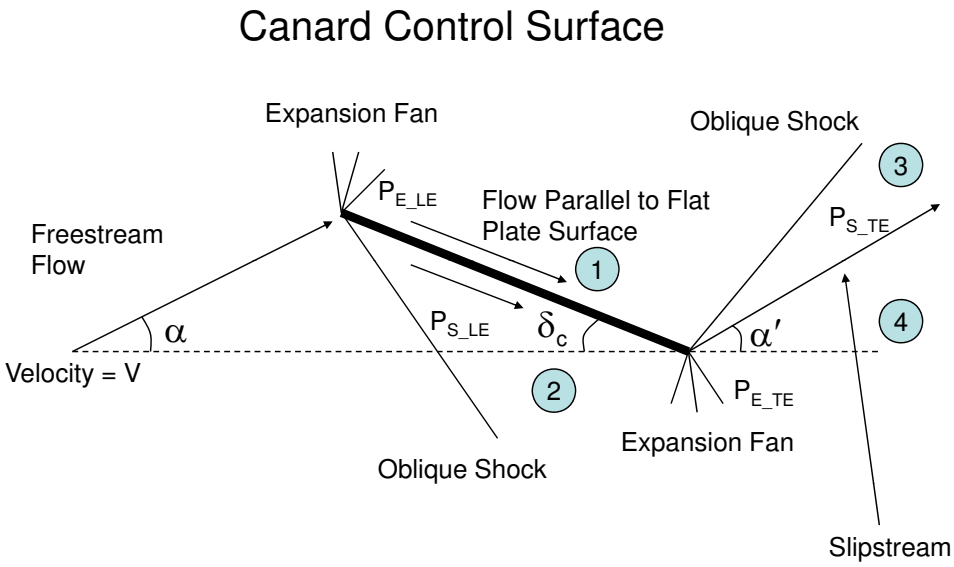

Figure 2. Flow Around Canard.

flow does not turn back parallel to the freestream but instead turns to a new angle, α'. The angle through which the flow turns at the rear of the flat plate self adjusts to equalize the pressures above and below the slipstream.

IV. Calculation Methods

The angle α' was calculated using two different techniques. The first utilizes an algorithm that solved the expansion and oblique shock equations for the angle (α') at which the flow pressures above and below the trailing edge of the canard are equal. The other used a Taylor's series expansion[2,3] relating the pressure change in the flow to the angle at which the flow turns. The goal was to determine how the new algorithm

compared with the approximation of the series method, as well as determine the number of series terms necessary for agreement between the two methods over the ranges of α and δ_c tested. When calculating the effects of the canard on the elevon, it was assumed that the slipstream would continue at the angle α' at which it left the trailing edge of the canard. The effects of flow mixing with the freestream are neglected in these two techniques.

A. Algorithm for Determination of α'

Two methods were utilized to determine the flow angle at the trailing edge of the canard, α'. The first method is denoted the "numerical technique", while the second method is called the "series solution". For the numerical technique, the code solves for the flow properties behind a shock or expansion using the nonlinear expressions for an oblique shock or an expansion fan. In the series methods, first- through fourth-order series expressions are used to determine the flow behind the shock or expansion fans.[1]

1. Numerical Technique

In the numerical technique, the flow properties behind an oblique shock or expansion fan are calculated numerically. For the oblique shock, the shock angle with respect to the freestream is a function of flow turn angle. The shock angle, θ_s, can be found be solving the following polynomial for $\sin^2\theta_s$:[5]

$$\sin^6\theta_s + b\sin^4\theta_s + c\sin^2\theta_s + d = 0 \tag{1}$$

where

$$\begin{aligned} b &= -\tfrac{M_\infty^2+2}{M_\infty^2} - \gamma\sin^2\delta \\ c &= \tfrac{2M_\infty^2+1}{M_\infty^4} + \left[\tfrac{(\gamma+1)^2}{4} + \tfrac{\gamma-1}{M_\infty^2}\right]\sin^2\delta \\ d &= -\tfrac{\cos^2\delta}{M_\infty^4} \end{aligned} \tag{2}$$

δ is the flow turn angle, commonly referred to as the wedge angle, M_∞ is the upstream Mach number, and γ =1.4 is the ratio of specific heats. The weak shock solution is selected as the answer. Once the shock angle has been found, the flow properties can be determined using[5]

$$\begin{aligned} \tfrac{p}{p_\infty} &= \tfrac{7M_\infty^2\sin^2\theta_s - 1}{6} \\ \tfrac{T}{T_\infty} &= \tfrac{\left(7M_\infty^2\sin^2\theta_s - 1\right)\left(M_\infty^2\sin^2\theta_s + 5\right)}{36M_\infty^2\sin^2\theta_s} \\ M^2\sin^2(\theta_s - \delta) &= \tfrac{M_\infty^2\sin^2\theta_s + 5}{7M_\infty^2\sin^2\theta_s - 1} \end{aligned} \tag{3}$$

where $M_\infty, p_\infty, T_\infty$ are the Mach number, static pressure, and static temperature upstream of the oblique shock and M, p, T are the Mach number, static pressure, and static temperature downstream of the oblique shock.

For flow over a convex corner, a Prandtl-Meyer expansion fan occurs. The first step here is to calculate the Prandtl-Meyer function, ν_∞:[6]

$$\nu_\infty = \sqrt{\frac{\gamma+1}{\gamma-1}}\tan^{-1}\sqrt{\frac{\gamma-1}{\gamma+1}\left(M_\infty^2-1\right)} - \tan^{-1}\sqrt{M_\infty^2-1} \tag{4}$$

The angle, ν, through which the flow is turned is $\nu = \nu_\infty + \delta$ where δ is the expansion ramp angle. To find the Mach number after the expansion, M, the following equation must be solved numerically

$$0 = \sqrt{\frac{\gamma+1}{\gamma-1}}\tan^{-1}\sqrt{\frac{\gamma-1}{\gamma+1}\left(M^2-1\right)} - \tan^{-1}\sqrt{M^2-1} - \nu_\infty \tag{5}$$

The remaining flow properties are calculated using isentropic flow relations[6]

$$\begin{aligned} \tfrac{p}{p_\infty} &= \left[\tfrac{1+\frac{\gamma-1}{2}M_\infty^2}{1+\frac{\gamma-1}{2}M^2}\right]^{\frac{\gamma}{\gamma-1}} \\ \tfrac{T}{T_\infty} &= \left[\tfrac{1+\frac{\gamma-1}{2}M_\infty^2}{1+\frac{\gamma-1}{2}M^2}\right] \end{aligned} \tag{6}$$

Given the freestream flow properties, α and δ_c, as inputs, the numerical technique calculates the flow properties on the top and bottom of the flat plate using the oblique shock and Prandtl-Meyer expansion fan equations discussed above. These calculations yield P_{E_LE} and P_{S_LE} along with the other flow properties in regions 1 and 2 of Figure 2. The notation is LE for leading edge and the subscripts E and S for flow behind an expansion fan or oblique shock. At this point, the flow has been turned parallel to the flat plate. The same oblique shock and expansion fan expressions are then used to determine the properties of the flow at the trailing edge of the canard in regions 3 and 4 of Figure 2. The objective is to find the trailing edge wedge angle, α', that yields equivalent upper and lower pressures at the trailing edge of the canard. In other words, referring to Figure 2, find α' such that $P_{E\_TE} = P_{S\_TE}$. This algorithm then iterates on this angle, such that the difference between the top and bottom pressures behind the canard, equals zero. The starting guess is taken to be the wedge angle $\alpha + \delta_c$. The outputs of the algorithm are the properties of the flow in regions 1, 2, 3, and 4 of Figure 2 along with the angle α'.

2. Series Method

Busemann[3] devised a method to find the turning angle of a flow passing through an expansion or an oblique shock using a Taylor series expansion, relating the pressure change to the turning angle of the flow. Busemann's[3] expression for the change in pressure is

$$\frac{p - p_\infty}{\frac{1}{2}\gamma p_\infty M_\infty^2} = \pm C_1(\delta) + C_2(\delta)^2 \pm (C_3 - D)(\delta)^3 + (C_4 - E)(\delta)^4 \tag{7}$$

where

$$C_1 = \frac{2}{\sqrt{M_\infty^2 - 1}} \tag{8}$$

$$C_2 = \frac{(M_\infty^2 - 2)^2 + \gamma M_\infty^4}{2(M_\infty^2 - 1)^2} \tag{9}$$

$$C_3 = \frac{M_\infty^4}{(M_\infty^2 - 1)^{\frac{7}{2}}} \left[\frac{\gamma + 1}{6} \left(M_\infty^2 - \frac{5 + 7\gamma - 2\gamma^2}{2(\gamma + 1)} \right)^2 + \frac{-4\gamma^4 + 28\gamma^3 + 11\gamma^2 - 8\gamma - 3}{24(\gamma + 1)} \right] + \frac{3(M_\infty^2 - \frac{4}{3})^2}{4(M_\infty^2 - 1)^{\frac{7}{2}}} \tag{10}$$

$$D = \frac{\gamma + 1}{12} \frac{M_\infty^4}{(M_\infty^2 - 1)^{\frac{7}{2}}} \left[\frac{(5 - 3\gamma)}{4} \left(M_\infty^2 - \frac{6 - 2\gamma}{5 - 3\gamma} \right)^2 - \frac{\gamma^2 - 1}{5 - 3\gamma} \right] \tag{11}$$

$$C_4 - E = \frac{\frac{3\gamma^3 - 3\gamma^2 - 7\gamma - 1}{24} M_\infty^{10} + \frac{3\gamma^3 - 3\gamma^2 + 33\gamma + 7}{24} M_\infty^8 + \frac{3\gamma^2 - 9\gamma - 2}{3} M_\infty^6 + \frac{8\gamma + 2}{3} M_\infty^4 - \frac{2}{3} M_\infty^2 + \frac{2}{3}}{(M_\infty^2 - 1)^5} \tag{12}$$

The quantity $C_4 - E$ was given in Hilton[7] (with $\gamma = 1.4$) as well as the method for the derivation of C_4 by itself.

For this method, the subscript ∞ refers to the conditions preceding the oblique shock or expansion wave and δ is the angle through which the flow turns. Initially, the flow is freestream, inclined at an angle α with respect to the body x-axis (see Figure 2). The turning angle for the leading edge of the flat plate is therefore $\delta_{LE} = \alpha + \delta_c$ where the subscript LE denotes leading edge. For the trailing edge, subscript TE, the flow turning angle is $\delta_{TE} = \alpha' + \delta_c$. The constants D and E are used only in the case of an oblique shock, which is non-isentropic. D and E are not included for the expansion fan calculations. The constants C_1, C_2, C_3, C_4 assume isentropic flow, such as is found in a Prandtl Meyer expansion. However, the non-isentropic losses become significant once the third-order term is reached, so it is necessary to include the constants D and E on the higher-order terms for the oblique shock case. Also, the upper sign in Eq. 7 is used on the upper surface, while the lower sign in Eq. 7 is used on the lower surface.

The pressures on the top and bottom of the canard are determined using this series with the known freestream properties and wedge angles. In order to find the turning angle at the rear of the flat plate, the expressions for the pressures above and below the slipstream behind the trailing edge were subtracted from each other and iterations on α' were performed until these pressures were equal. In other words, the angle α' was found such that the pressures in regions 3 and 4 of Figure 2 were equal.

B. Method Comparison

Both of the methods were utilized to find α' for cases with δ_c ranging from $-20°$ to $+20°$ and α ranging from $-1°$ to $5°$. For the series method, different orders of approximations were used, ranging from first to fourth. The different order series, referring to Eq. 7, are defined as

$$\begin{aligned} First - Order &: \frac{p-p_\infty}{\frac{1}{2}\gamma p_\infty M_\infty^2} = \pm C_1(\delta) \\ Second - Order &: \frac{p-p_\infty}{\frac{1}{2}\gamma p_\infty M_\infty^2} = \pm C_1(\delta) + C_2(\delta)^2 \\ Third - Order &: \frac{p-p_\infty}{\frac{1}{2}\gamma p_\infty M_\infty^2} = \pm C_1(\delta) + C_2(\delta)^2 \pm (C_3 - D)(\delta)^3 \\ Fourth - Order &: \frac{p-p_\infty}{\frac{1}{2}\gamma p_\infty M_\infty^2} = \pm C_1(\delta) + C_2(\delta)^2 \pm (C_3 - D)(\delta)^3 + (C_4 - E)(\delta)^4 \end{aligned} \tag{13}$$

Figures 3 - 6 show the values of α' versus δ_c for the first- through fourth-order series methods. The solid lines in these figures correspond to the α' values calculated with the numerical technique, while the dashed lines correspond to α' values calculated with the series method. Clearly, the first-order method poorly estimates α' for wedge angles larger than about $3°$ (see Figure 3). Likewise, the second-order method is only accurate for wedge angles of about $3°$. The third-order series method (Figure 5) produced acceptable results for α' for wedge angles up to around $7°$. The fourth-order series method is quite accurate up to about $13°$.

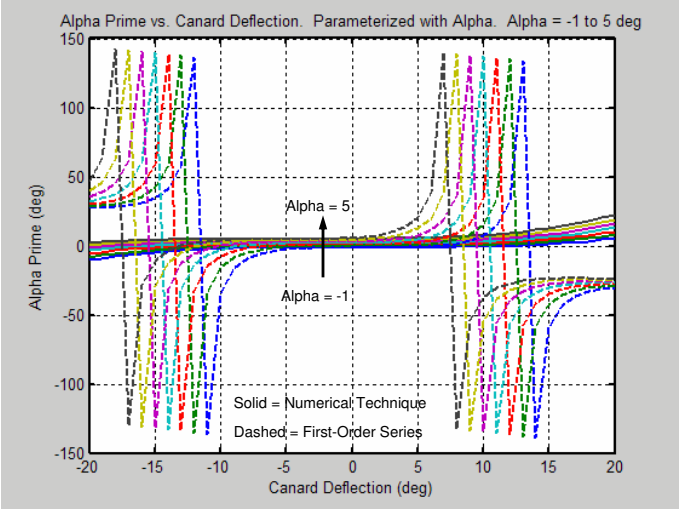

Figure 3. α' for Numerical Technique (Solid Lines) and First-Order Series Method (Dashed Lines)

The issue with the differences between α' computed with the two techniques is simply the difference in calculations of pressures behind a shock or expansion for the two methods. As the order of the series increases, the calculation of surface pressures more closely matches the results from numerically solving the oblique shock/expansion fan equations. Figure 7 shows the pressure on the lower surface of the canard as computed using the first- and fourth-order series method expansion fan/shock calculations and the expansion fan/shock relationships in Eqs. 4 - 6 and Eqs. 1 - 3. Figure 8 shows the results for the upper surface of the canard. Again, the first-order series method poorly computes the pressures behind the expansion fan and shock. Increasing the order of the series can yield significant improvements, as the fourth-order series method more closely resembles the numerical calculations. The differences in α' between the series and numerical methods is a direct result of the pressures being calculated differently. In fact, Figures 7 and 8 only show part of the story. The flow is turned through an expansion and shock at the rear of the canard also, so these series calculations are performed again and the errors increase. Figure 9 shows the pressures below and above the slipstream behind the canard as computed using the first-order series method and the numerical technique. The errors in the calculation at the leading edge of the canard have propagated and the pressures, as computed by the two methods, are much different. When computing α', the pressures below and above the slipstream are equated. Because the pressures calculated using the series method and those calculated using the numerical technique differ, the α' values differ. Similar results occur when the fourth-order series

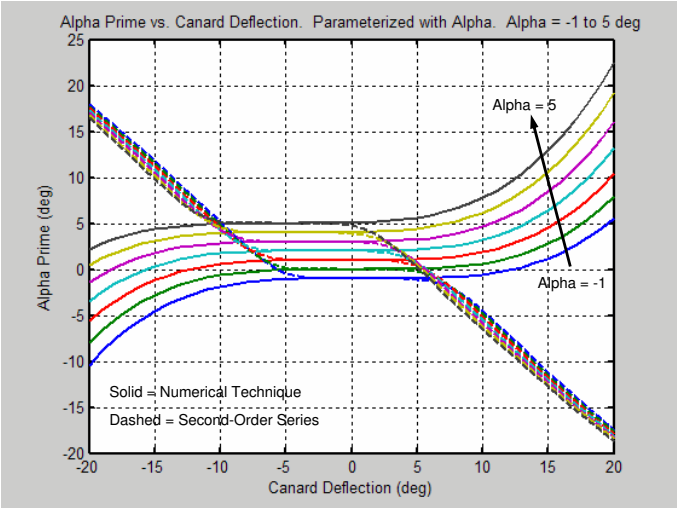

Figure 4. α' **for Numerical Technique (Solid Lines) and Second-Order Series Method (Dashed Lines)**

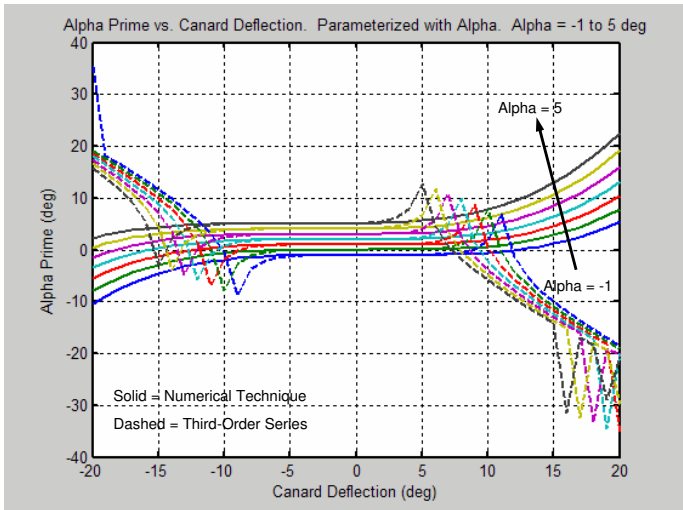

Figure 5. α' **for Numerical Technique (Solid Lines) and Third-Order Series Method (Dashed Lines)**

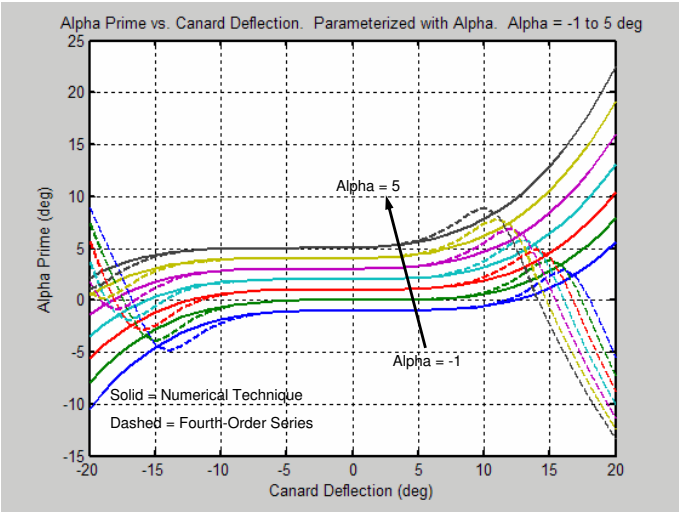

Figure 6. α' **for Numerical Technique (Solid Lines) and Fourth-Order Series Method (Dashed Lines)**

method is used, as shown in Figure 10. As was the case with the leading edge, the fourth-order series method is more accurate than the first-order series method, but differences do exist when compared to the numerical calculations.

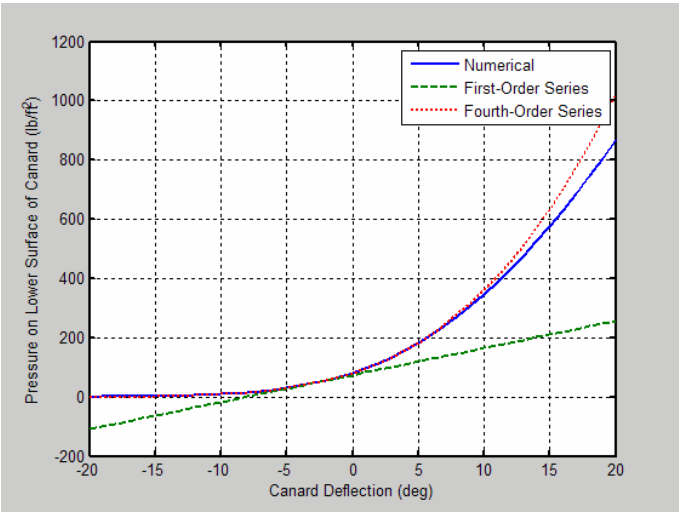

Figure 7. Pressure on Lower Surface of Canard - Numerical, First-Order Series, and Fourth-Order Series.

V. Elevon Control Surface

This slipstream effect must be taken into account in order to determine the flow on the elevon control surface. The geometry of the interaction is shown in Figure 11. In Figure 11, α'_{max} and α'_{min} are the maximum and minimum angles, measured from the horizontal, at which the slipstream can come off the canard and strike the elevon. They can be expressed in terms of the other vehicle dimensions with the following equations:

$$\alpha'_{max} = \arctan\left[\frac{Z_{elev} + \frac{1}{2}L_c \sin\delta_c + \frac{1}{2}L_e \sin\delta_e}{X_{canard} + X_{elev} - \frac{1}{2}L_c \cos\delta_c - \frac{1}{2}L_e \cos\delta_e}\right] \tag{14}$$

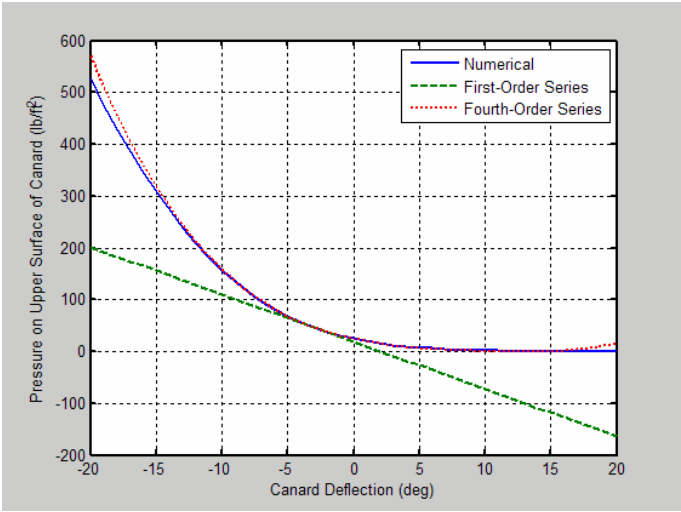

Figure 8. Pressure on Upper Surface of Canard - Numerical, First-Order Series, and Fourth-Order Series.

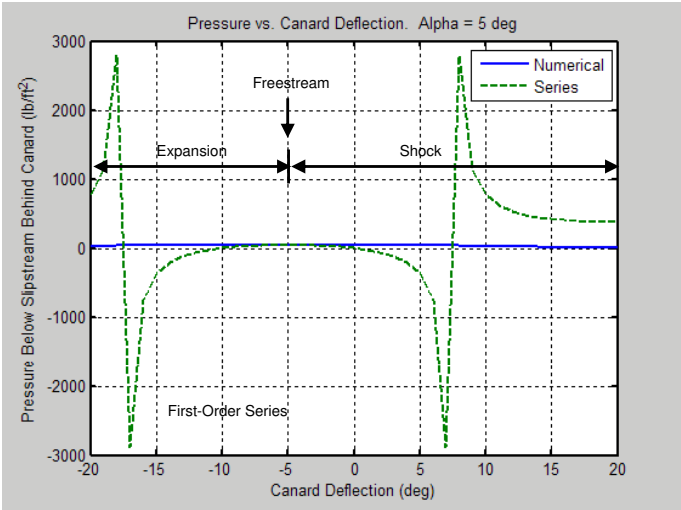

Figure 9. Pressure Below and Above Slipstream - Numerical and First-Order Series.

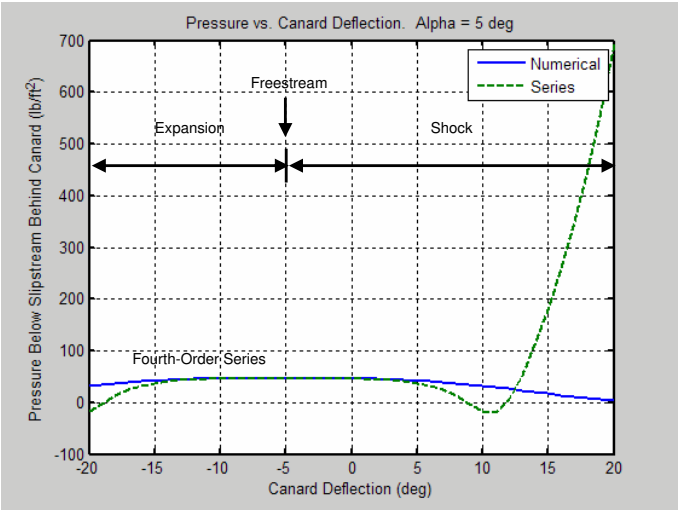

Figure 10. Pressure Below and Above Slipstream - Numerical and Fourth-Order Series.

$$\alpha'_{min} = \arctan\left[\frac{Z_{elev} + \frac{1}{2}L_c \sin\delta_c - \frac{1}{2}L_e \sin\delta_e}{X_{canard} + X_{elev} - \frac{1}{2}L_c \cos\delta_c + \frac{1}{2}L_e \cos\delta_e}\right] \tag{15}$$

Recall, it is assumed that the flow seen by the elevon is the flow leaving the trailing edge of the canard. Hence, no mixing of the flow, at the trailing edge of the canard, with freestream flow occurs.

Figure 12 shows the geometry of the flow incident upon the elevon. When $\alpha' > \alpha'_{max}$, the flow incident upon the elevon is the flow below the slipstream at the trailing edge of the canard. When $\alpha' < \alpha'_{min}$, the flow incident upon the elevon is the flow above the slipstream at the trailing edge of the canard. When $\alpha'_{min} \leq \alpha' \leq \alpha'_{max}$, the slipstream impinges upon the elevon. In this case, if $\delta_e > -\alpha'$, the elevon experiences the flow above the slipstream. On the other hand, if $\delta_e < -\alpha'$, the elevon experiences the flow below the slipstream. The algorithm to determine the flow properties on the elevon is as follows:

1. If $\alpha' > \alpha'_{max} \Rightarrow$ Incident flow on elevon = Flow ***BELOW*** slipstream
2. If $\alpha' < \alpha'_{min} \Rightarrow$ Incident flow on elevon = Flow ***ABOVE*** slipstream
3. If $\alpha'_{min} \leq \alpha' \leq \alpha'_{max} \Rightarrow$ Check additional condition. If $\delta_e > -\alpha' \Rightarrow$ Incident flow on elevon = Flow ***ABOVE*** slipstream, If $\delta_e < -\alpha' \Rightarrow$ Incident flow on elevon = Flow ***BELOW*** slipstream

Oblique shock and expansion fan computations are used, with the initial flow properties discussed above, to compute the flow properties on the top and bottom surfaces of the elevon. The ultimate goal is to determine how the flow leaving the canard effects the elevon. In the next section, the elevon effectiveness is calculated.

VI. Elevon Effectiveness

Now that the flow properties at the elevon have been calculated, the effectiveness of the elevon can be determined. To begin, the static pressures on the top and bottom of the elevon are integrated to determine the forces due to this control surface. Moreover, since the elevon is primarily used for attitude control, the pitching moment due to these forces is calculated. Recall, the goal is to determine the effects of the upstream canard control surface on the moment generating effectiveness of the elevon. Figure 13 shows the moment ratio produced by the elevon when the canard flow is incident upon the elevon for two different angles of attack ($\alpha = -1^\circ$ and $\alpha = 5^\circ$). The moment ratio is defined as the moment generated by the elevon due to the disturbed flow from the canard divided by the moment the elevon would generate if the elevon experienced freestream flow. It should be pointed out that, if freestream flow impinges the elevon, the moment produced is independent of canard deflection. Clearly, as the effective wedge angle of the canard increases, the moment produced by the elevon decreases when compared to the one it would generate with freestream conditions.

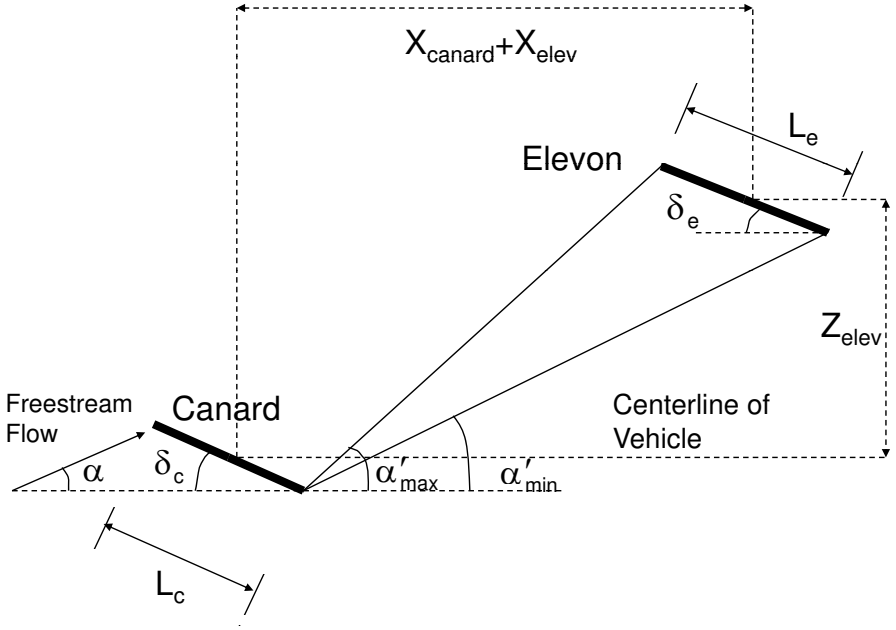

Figure 11. Geometry for Flow on Elevon.

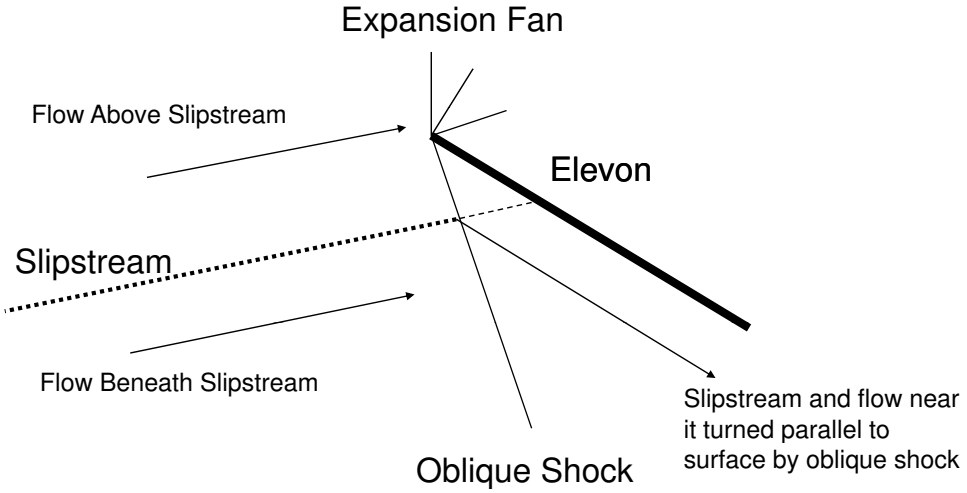

Figure 12. Slipstream-Elevon Interaction Diagram.

Hence, the elevon becomes less effective as the flow turn angle for the upstream control effector increases. In Figure 13, the sharp change in moment from $\delta_c = -19°$ to $\delta_c = -18°$ is due to the incident flow on the elevon changing from flow above the slipstream when $\alpha = 5°, \delta_c = -19°, \delta_e = 8°$ to flow below the slipstream when $\alpha = 5°, \delta_c = -18°, \delta_e = 8°$.

This result shows that when the effects of the canard are taken into account on the elevon, a significant decrease in moment produced by the elevon can result. These effects are directly seen in terms of elevon effectiveness. The elevon effectiveness is defined as the change in moment produced by the elevon per change in elevon deflection, i.e.,

$$\frac{dM_e}{d\delta_e} = \frac{M_e\left(Mach, \alpha, \delta_c, \delta_{e_i}\right) - M_e\left(Mach, \alpha, \delta_c, \delta_{e_{i-1}}\right)}{\delta_{e_i} - \delta_{e_{i-1}}} \tag{16}$$

Thus, the elevon effectiveness is computed using a finite difference. This result can be normalized by the control effectiveness of the elevon if it were subjected to freestream flow conditions (and, therefore, independent of canard deflection), such that

$$ElevonEffectivenessRatio = \frac{\frac{\partial M_e}{\partial \delta_e}}{\frac{\partial M_e}{\partial \delta_e}|_\infty} \tag{17}$$

Figure 14 shows the elevon effectiveness ratio for $\delta_e = 8°$ and angles of attack of $-1°$ and $5°$. As expected, for large canard wedge angles, the effectiveness of the elevon decreases significantly when the flow from the canard is incident upon the elevon, as compared to assuming freestream flow incident upon the elevon.

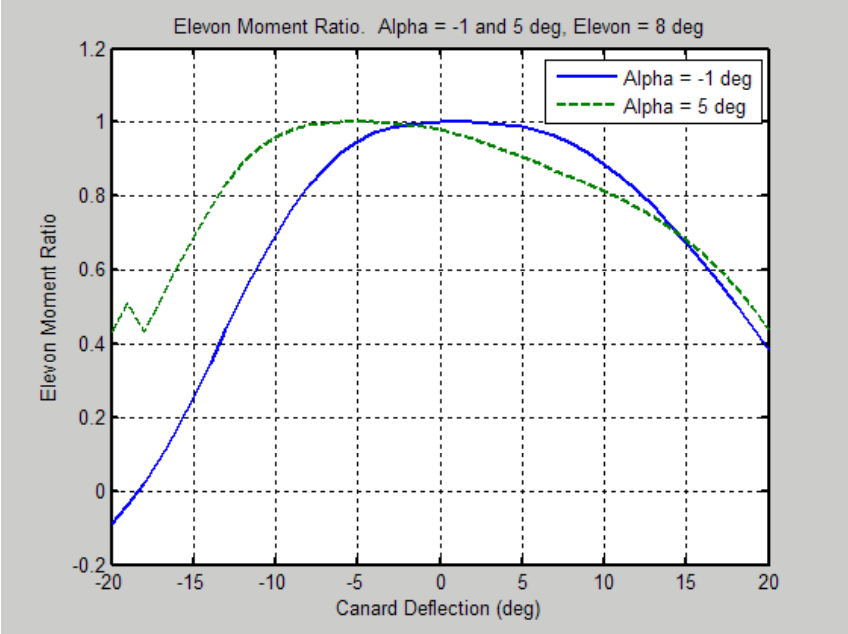

Figure 13. Elevon Moment Ratio: Elevon Deflection = 8°

VII. Conclusions

In this work, the interaction between two control surfaces, on downstream of another, was investigated. Comparisons were made between Busemann's[3] series approximation for flow behind an oblique shock or expansion fan and the actual calculations from the nonlinear flow relations. For small wedge angles, these two methods produced similar results. In order to determine the flow behind the canard, a pressure balance was performed downstream of the trailing edge of the canard. A slipstream forms with different velocity flow above and below. It was assumed that the flow properties incident upon the elevon were the flow properties

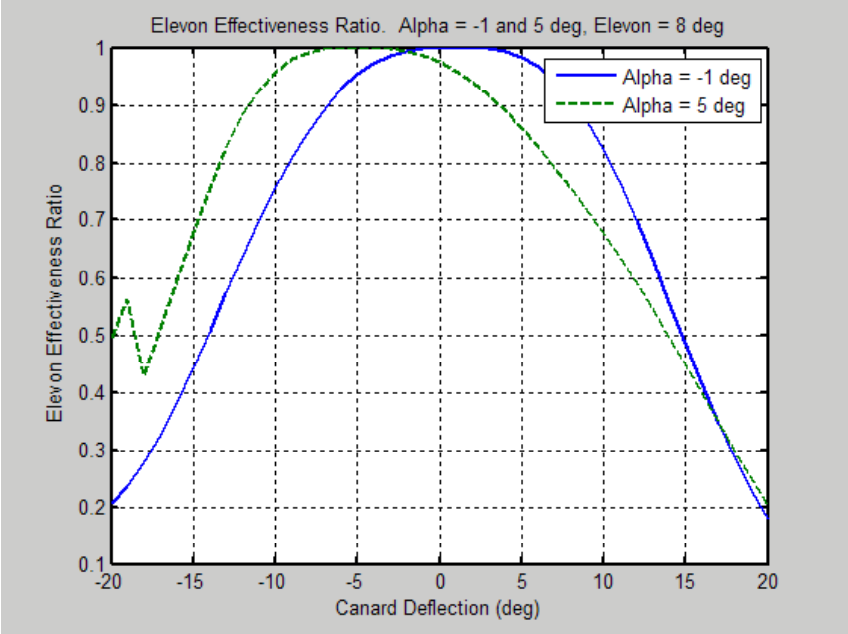

Figure 14. Elevon Effectiveness Ratio: Elevon Deflection = 8°

downstream of the canard. The results show that the slipstream from the trailing edge of the canard can have significant interaction effects with the elevon. The primary effect is a decrease in elevon effectiveness. These interactions have the potential to complicate the blending and mixing of the control effectors for this class of vehicle. The relative placement of the effectors have significant impact upon the controllability and interaction effects should be considered early in the vehicle design phase.

References

[1]Kahane, A. and Lees, L., "The Flow at the Rear of a Two-Dimensional Supersonic Airfoil," *Journal of the Aeronautical Sciences*, 1948, pp. 167–170.

[2]Lighthill, M. J., "The Conditions Behind the Trailing Edge of the Supersonic Airfoil," *Reports and Memoranda No. 1930*, 1944, pp. 249–256.

[3]Busemann, A., "Aerodynumischer Auftrieb bei Uberschallgeschwindigkeit," *Luftfahrtforschung*, Vol. Band 12, No. 6, 1935.

[4]Oppenheimer, M. W., Skujins, T., Bolender, M. A., and Doman, D. B., "A Flexible Hypersonic Vehicle Model Developed with Pistion Theory," *Proceedings of the 2007 Guidance, Navigation and Control Conference*, AIAA 2007-6396, August 2007.

[5]"Equations, Tables, and Charts for Compressible Flow," Tech. Rep. Tech. Rep. NACA-1135, National Advisory Committee for Aeronautics, Ames Aeronautical Laboratory, Moffett Field, CA, 1953.

[6]Anderson, J. D., *Fundamentals of Aerodynamics*, McGraw-Hill, Inc., 1984.

[7]Hilton, W., *High-Speed Aerodynamics*, Longmans, Green, and Co., New York, 1951.